Nd:MgO:LiNbO₃ spectroscopy and laser devices

T. Y. Fan, A. Cordova-Plaza, M. J. F. Digonnet,* R. L. Byer, and H. J. Shaw

Edward L. Ginzton Laboratory, W. W. Hansen Laboratories of Physics, Stanford University, Stanford, California 94305

Laser oscillation in Nd:MgO:LiNbO₃ has been demonstrated. Thresholds as low as 3.6 mW and slope efficiencies up to 39% were achieved in a resonantly pumped miniature device. The electro-optical and nonlinear-optical properties of the host were also used to make active internal Q-switched and self-frequency-doubled lasers. Photorefractive damage is shown to be greatly suppressed compared with that for non-MgO-doped material. Absorption spectra, fluorescence spectra, and lifetime measurements are also reported.

1. INTRODUCTION

Nd-doped LiNbO₃ is a promising laser material that combines the excellent laser properties of the Nd^{3+} ion with the electro-optical and nonlinear-optical properties of lithium niobate. This permits the design of interesting yet simple devices, including self-frequency-doubled lasers, self-Q-switched and self-modulated lasers, and waveguide devices.

The first laser oscillation in Nd:LiNbO₃ was reported in 1967.[1] Subsequently several research groups studied the absorption and fluorescence spectra and the energy levels of this material[2-5] and investigated both flash-lamp-pumped[3,6,7] and laser-pumped Nd:LiNbO₃ lasers.[8,9] Self-frequency doubling was originally demonstrated in Tm:LiNbO₃[3] and later in Nd:LiNbO₃.[10] However, the photorefractive effect in LiNbO₃ appeared to reduce greatly the efficiency and usefulness of the devices that involved short-wavelength radiation.

Several years ago Zhong *et al.*[11] showed that LiNbO₃ doped with approximately 5% or more magnesium oxide exhibits a remarkably reduced photorefractive response compared with undoped LiNbO₃. This highly MgO-doped material has been used to make Q switches and frequency doublers.[12] MgO doping of Nd:LiNbO₃ was previously used to increase the distribution coefficient of Nd into LiNbO₃.[7] Yet no reduction of the photorefractive effect was noted, most likely because of a low MgO concentration. In view of the previous work and more recent studies,[13] it was interesting to investigate the properties of Nd:MgO:LiNbO₃ as a potentially high-damage-threshold laser material.

Recently we reported successful laser operation and self-frequency doubling in this material[8] as well as self-Q-switched laser operation.[14] In this paper we give a more thorough description of our investigation of the properties of Nd:MgO:LiNbO₃ as well as of several laser devices. In Sections 2 and 3 we discuss the material properties and spectroscopy, respectively. This is followed in Section 4 by the description of quasi-cw and cw room-temperature lasers. In Section 5 we characterize the resistance of these devices to photorefractive damage. Finally, self-frequency doubled and self-Q-switched laser operation are described in Sections 6 and 7.

2. MATERIAL

LiNbO₃ is a uniaxial crystal that belongs to the space group C_{3v}^6. Nd^{3+} can substitute into either the Li^+ or the Nb^{5+} site[15]; both sites are on the C_{3v} axis and are characterized by C_{3v} site symmetry. Neither substitution site lies on an inversion center, so electric-dipole transitions should be allowed.

The samples used in this work were cut from two boules grown and provided to us by Crystal Technology. Both boules were grown from originally congruent Li/Nb ratio melts into which 5-mol. % MgO and 0.5–1.0-at. % Nd were added. Emission spectroscopy analysis indicates that both boules contained 2.5-wt. % MgO. They were also doped with 0.15- and 0.2-wt. % Nd₂O₃ and will be referred to as the low- and high-doped samples, respectively. The ratio of Nd concentrations was confirmed by optical absorption measurements. Both samples were grown along the crystal z axis. They exhibited striations perpendicular to this direction, which were quite visible to the naked eye, with a period of the order of 0.2 mm for the low-doped sample and 0.5–1.0 mm for the high-doped sample. The most likely explanation for these striations is a variation in the material refractive index induced by composition variations, in particular changes in the Li/Nb ratio and/or in the Mg concentration. In addition, the higher-Nd-doped sample exhibited a large number of inclusions. However, as we shall see, we were able to demonstrate remarkably low-loss devices with these early samples. Further loss reduction is expected in future generation crystals.

3. SPECTROSCOPY

The fluorescence lifetimes, absorption spectra, and fluorescence spectra have been investigated. The fluorescence lifetimes were measured by pumping the samples with a frequency-doubled Q-switched Nd:YAG laser. A long-pass filter was used to block the pump light and pass the near-infrared fluorescence from the sample. The signal was monitored with a silicon detector and then displayed on an oscilloscope. The measured lifetimes were 120 and 102 μsec at room temperature for the low-doped and high-doped sam-
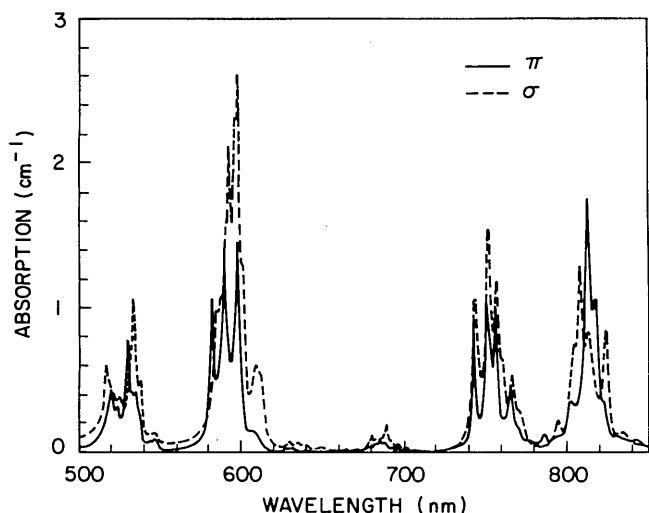
Fig. 1. Absorption coefficient as a function of wavelength for the high-doped sample.
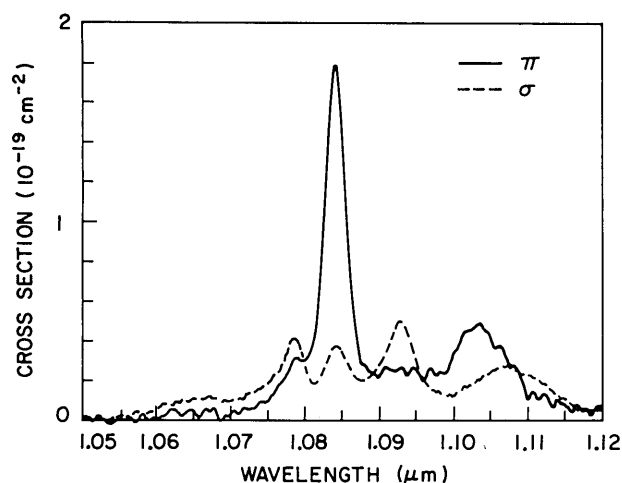

Fig. 2. Effective stimulated-emission cross section calculated from the fluorescence spectrum.

ples, respectively. Previous reports indicated lifetimes in the 80–85-μsec range for 1-wt. % Nd samples[2] and 100 μsec for 0.5-wt. % Nd samples.[9] These results indicate concentration quenching. In addition, no change in lifetime was measured in the high-doped sample for temperatures up to 100°C. This is consistent with other measurements of the temperature dependence of the Nd^{3+} fluorescence lifetime in other single-crystal hosts (YAG, YAlO₃).[16] The fluorescence decay was exponential in character even though the Nd^{3+} ions occupy two different substitutional sites in $LiNbO_3$. In general, the two sites would be characterized by different lifetimes, which would lead to a nonexponential fluorescence decay. However, based on the exponential fluorescence decay, it appears that the two sites must have nearly equivalent lifetimes.

The absorption spectra for both the π ($E\|c$) and σ ($E\perp c$) polarizations are shown in Fig. 1 for the 0.2-wt. % Nd_2O_3 sample. These spectra were measured using a Perkin-Elmer 330 spectrophotometer with a resolution of 0.9 nm and a calcite polarizer to separate polarizations.

The fluorescence spectra were measured using a Rhodamine 590 dye laser to excite the Nd:MgO:LiNbO₃, a Chroma-

tix Model CT 103 monochromator and a calcite polarizer to analyze the spectra, and a germanium detector. The spectra were digitally recorded and corrected for the relative response of the detection system. The fluorescence spectra near 1.09 μm are similar to previously published data.[3,5] The spectrum of the $E\perp c$ (or σ) polarization was found to be identical to the axial spectrum for both the absorption and the fluorescence, which indicates that the transitions involved are electric-dipole in nature, as expected.

From the fluorescence spectra, the effective stimulated emission cross section can be calculated by using the following equation[17,18]:

$$\sigma_e^p(\lambda) = \frac{3\lambda^5 \beta_j I^p(\lambda)}{8\pi n^2 c \tau_R \int \lambda I(\lambda) d\lambda} , \qquad (1)$$

where λ is the signal wavelength, n the material refractive index, c the speed of light, τ_R the radiative lifetime of upper laser level, and $I^p(\lambda)$ the light intensity as a function of wavelength. The superscript p denotes either state of polarization. The integral in the denominator is performed over the fluorescence in all polarizations between the manifolds of interest, in this case $^4F_{3/2}$–$^4I_{11/2}$. The branching ratio β_j is defined to be

$$\beta_j = \frac{\int \lambda I_j(\lambda) d\lambda}{\sum_i \int \lambda I_i(\lambda) d\lambda} , \qquad (2)$$

where the integral in the numerator is calculated from the upper laser level to the manifold of interest and the sum in the denominator is carried out over fluorescence from the upper laser level to all lower-lying manifolds ($^4I_{15/2}$, $^4I_{13/2}$, $^4I_{11/2}$, and $^4I_{9/2}$). The branching ratio for $^4F_{3/2}$–$^4I_{11/2}$ has been measured to be 0.44.[19] Using Eq. (1) and the assumption that the radiative lifetime is 120 μsec (i.e., unity radiative quantum efficiency), the effective stimulated-emission cross section can be calculated. The results are shown in Fig. 2. The peak cross section calculated by this method is near $\sigma_e = 1.8 \times 10^{-19}$ cm² for the π polarization and 5.1×10^{-20} cm² for the σ polarization compared with previously measured values of 5×10^{-19} cm² and 2×10^{-19} cm², respectively.[5]

The linewidths of the transitions are substantially greater than those in Nd:YAG. This can most likely be attributed to the two distinct sites for the Nd^{3+} ion, which have slightly different energy levels.[2] Although two separate sets of transitions that are due to the two different sites cannot be observed at room temperature, it was previously noted that at lower temperatures, 77 K, double peaks in the transitions can be observed, indicating differences in transition energies for the two sites in the 10–20-cm⁻¹ range.[2]

4. CONTINUOUS-WAVE LASER OPERATION

System Description
Continuous-wave and quasi-cw room-temperature laser operation was achieved in four samples of Nd:MgO:LiNbO₃. Two of these samples were cut along the y axis, so that laser oscillation was obtained preferentially in the high-gain or π polarization at a wavelength of 1.085 μm. The other two crystal rods were oriented along the z axis. In these samples laser action could be achieved only in the low-gain polariza-
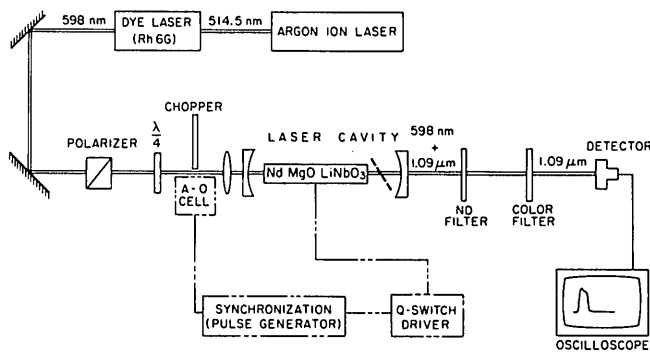
Fig. 3.   Schematic of the miniature Nd:MgO:LiNbO$_3$ laser experimental arrangement. (ND, neutral density.)

tion at $\lambda = 1.093\ \mu m$. Since the axial spectrum was shown to be the same as the σ spectrum, the low-gain polarization will be referred to as the σ polarization. The two y-cut rods, with dimensions 2 mm × 2 mm × 10 mm, as well as one of the z-cut rods (1 mm × 1 mm × 5 mm) had their end faces antireflection coated with 1875 Å of SiO$_2$. The second z axis rod (2 mm × 2 mm × 11.5 mm) had its ends antireflection coated with multidielectric layers. All samples were of the low-doped type.

The experimental arrangement used for the laser measurements is illustrated in Fig. 3. It consists of the pump lasers, the Nd:MgO:LiNbO$_3$ laser cavity, and the detection elements. The components shown by dashed lines were incorporated only for Q-switched operation.[14] The pump laser was a cw Rhodamine 6G dye laser tuned to the 598-nm absorption line of the material. To reduce measurement errors owing to feedback, we optically isolated the miniature laser cavity from the pump laser, as shown in Fig. 3.

To minimize degradation resulting from the residual photorefractive effect in the material, the pump beam was chopped to reduce its duty cycle to ~1.2%. The crystals were thus pumped with ~500-μsec-long pulses at a repetition rate of 25 Hz. The pulse width was chosen to be more than four times the fluorescence lifetime of the material to be in the quasi-cw mode.

Miniature Laser Cavity Design

The first criterion in the design of the miniature laser cavity was the minimization of the pump threshold power by properly choosing the lens and cavity parameters. From the formalism of mode overlap[20,21] an approximate expression can be derived for the pump power P_{th} that needs to be absorbed by the material to reach oscillation threshold:

$$P_{th} = \frac{h\nu_p}{\sigma\tau_f}\frac{\delta}{2}\left[\frac{\pi}{2}(\bar{w}_p{}^2 + \bar{w}_s{}^2)\right]. \qquad (3)$$

where ν_p is the pump frequency, σ the net-gain cross section, τ_f the fluorescence lifetime, and δ the round-trip cavity loss including output coupling. $\bar{w}_p$ and $\bar{w}_s$ are the average pump- and signal-mode radii averaged along the length of the crystal.[21] The net-gain cross section σ is the difference between the effective stimulated-emission cross section σ_e [Eq. (1)] and the excited-state absorption (ESA) cross section. The latter parameter has not been measured in this material, but we believe that the ESA cross section is small, and we will treat σ and σ_e as the same parameter.

From Eq. (3) it is clear that for a given material the threshold is minimum when both the average signal- and pump-mode areas inside the crystal are minimized. The average mode radii can be simply calculated by integrating the well-known Gaussian-beam propagation equation over the crystal length as follows:

$$\bar{w}_i{}^2 = \frac{w_i{}^2}{l}\int_0^l\left\{1 + \left[\frac{\lambda_i(z - z_i)}{\pi w_i{}^2 n}\right]^2\right\}dz. \qquad (4)$$

In this expression, the subscript i refers to pump (p) or signal (s), w_i is the beam-waist radius, z_i is the location of this waist inside the crystal where $z = 0$ at the input face of the crystal, and l is the crystal length.

The value of w_i that minimizes $\bar{w}_i$ is equal to

$$\omega_{i,opt} = \left(\frac{\lambda_i l}{\sqrt{12}\pi n}\right)^{1/2}, \qquad (5)$$

where λ_i is the pump ($i = p$) or signal ($i = s$) wavelength.

From resonator Gaussian-mode theory it can be shown that for given mirror curvatures there are two cavity lengths L that realize condition (5). With the mirrors that were available to us, the first of these lengths corresponded to cavities that were shorter than our crystals and therefore not physically realizable. The smallest practical signal waist obtainable with a short cavity is achieved when $L = l$. This configuration will be referred to hereafter as the minimum-length cavity. The second solution is very close to the so-called spherical-cavity configuration, which is at the edge of the stability region. Therefore, as a compromise between minimum threshold and mechanical stability, slightly smaller lengths than this optimum were selected. This type of cavity configuration is referred to as the nearly concentric cavity.

A similar analysis was carried out to optimize the pump-waist radius through the selection of the optimum focal length for the focusing element. The pump-beam diameter was accurately measured just before the miniature laser cavity by using a Reticon linear detector array. An $f = 10.0$-cm lens was then selected to provide near-optimum pump-waist radii inside the crystal.

Experimental Results

Both nearly concentric cavities and minimum-length cavities were investigated in this work, the former because of
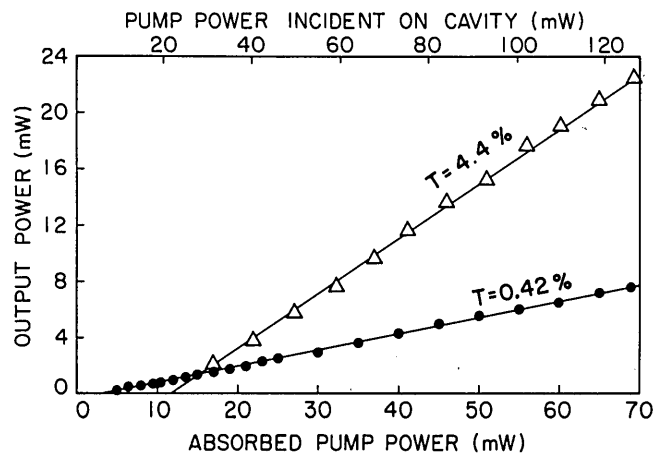

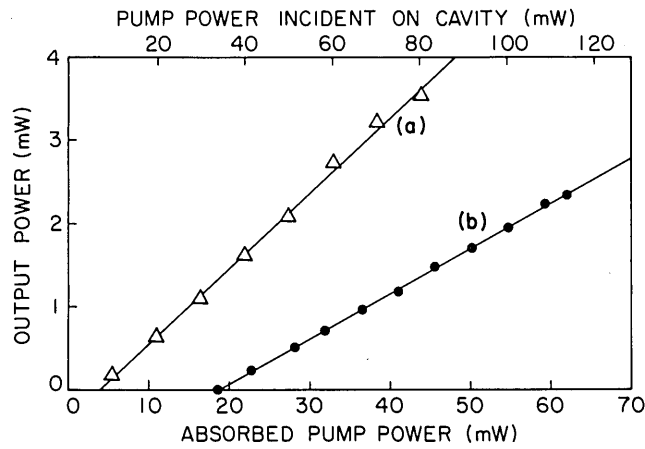Fig. 4.   Output-power versus pump-power curves, π polarization.

Fig. 5. Output-power versus pump-power curves, σ polarization. (a) $R = 5$ cm, $L = 106$ mm, $T = 0.42\%$. (b) $R = 10$ cm, $L = 6.5$ mm, $T = 0.30\%$.

Table 1. Continuous-Wave Laser Data

Polar-ization	Crystal	T (%)	Slope Efficiency (%)	Inferred Crystal Loss (%)	Threshold Power (mW)
π	y axis	4.4	39	1.8	12
π	y axis	0.42	11.7	1.6	3.6
σ	z axis	0.42	9.05	2.1	3.9
σ	z axis	0.3	5.4	2.7	18.8

their inherent lower threshold and the latter because they provide a way to estimate the net-gain cross section of the material.

Figure 4 shows plots of the laser output power at $\lambda = 1.085$ μm versus absorbed pump power for y-cut lasers in a short cavity. The first laser consisted of two 5-cm-radius mirrors, a high reflector, and a 0.42% transmissive output coupler separated by a distance of 11.5 mm. The second laser was identical, except that the output coupler was 4.4% transmissive with a 10-cm radius of curvature. The oscillation thresholds are relatively low, of the order of 4 to 12 mW. As expected, the output grows linearly with the absorbed pump power. A least-squares fit to a straight line was made to the experimental data (solid lines in Fig. 4). The device slope efficiency is defined as the slope of the curve fits, i.e., as the ratio of output energy to input energy above threshold. The slope efficiency of 39% observed with the high-transmission output coupler is close to the theoretical limit of 55% given by the ratio of signal to pump photon energy. A maximum quasi-cw output power in excess of 22 mW was observed for an absorbed pump power of 70 mW, which corresponds to a maximum available pump power incident upon the laser cavity of 128 mW.

Note that the analysis presented previously predicted a pump-power threshold much smaller for a nearly concentric cavity than for a minimum length cavity. This was verified experimentally by increasing the mirror separation up to 10.4 cm in the laser having a 0.42% transmissive output coupler. Under these conditions the absorbed pump power required to reach threshold was lower than 1 mW. However, the short-term power fluctuations of this laser, about 3 to 6%, were larger than those for the short-cavity lasers, which

were typically 1%. The better stability of the short laser is probably attributable to the less severe influence of pump-beam wandering because of the much larger signal-mode size.

Figure 5 shows the output power characteristic of two low-gain, z-cut lasers. The first one was made of the longer crystal in a nearly concentric cavity. This laser was run cw without noticeable output degradation during the time it took to characterize it. To the best of our knowledge this is the first report of cw oscillation in Nd:LiNbO$_3$. Because of the smaller mode size in this device, its threshold was comparable with that of the previous high-gain devices, of the order of 4 mW. The second laser was made of the short crystal placed in a short cavity. The larger mode size is responsible for its higher threshold. The data for the lasers of Figs. 4 and 5 are summarized in Table 1.

In all miniature lasers the transverse mode structure of the signal beam was carefully analyzed with a Reticon linear detector array. Under optimum threshold conditions, all lasers were found to oscillate in the fundamental Gaussian mode. The measured beam diameter served to determine the signal-waist radius inside the cavity by using standard matrix formalism. The signal-waist radii obtained by this method agree to better than 10% with theoretical predictions from the cavity parameters. The waist radii were typically 70 μm for short-cavity lasers and about 34 μm for the nearly concentric-cavity laser. By comparing these figures with the optimum value predicted by Eq. (5) it can be seen that the threshold could be further reduced. The pump-waist radii were about 20 μm for the short cavities and 29 μm for the nearly concentric laser.

Determination of δ and σ

The theoretical analysis given in Ref. 22 indicate that above threshold the laser output P_{out} of a four-level system grows linearly with the input pump power with a slope efficiency defined as $s = P_{out}/(P_{abs} - P_{th})$. For relatively low round-trip losses this slope efficiency may be approximated by[23]

$$s \simeq \frac{T}{\delta} \frac{h\nu_s}{h\nu_p}, \qquad (6)$$

where P_{abs} is the absorbed pump power and T is the output coupling.

This relation was used to calculate the round-trip cavity loss and the material cross section σ from the measurable laser quantities P_{th} and s. The laser loss δ was obtained directly from the measured slope efficiency by using relation (6). The measured pump- and signal-waist radii were replaced in Eq. (4) to yield the average waist radii inside the crystal rod. With these values and the cavity loss, δ, σ was determined with the help of Eq. (3).

When the waist radii are small (30 μm or less), the error introduced on σ may be significant. For this reason, in calculating σ we used only data from the short-cavity lasers, for which $w_s \sim 70$ μm. In addition, for these cavities the pump-waist radius was much smaller than the signal-waist radius, and an error in w_p had less severe influence in the determination of σ.

The residual crystal loss figures inferred from relation (6) are listed in Table 1. They are defined as the excess loss $\delta - T$ and therefore include crystal loss and antireflection-coating spurious reflections. These losses, of the order of

1%/cm, indicate that the crystals used exhibited relatively small losses despite the optical defects that they contained. The values of the effective gain cross section deduced by the method described above are $\sigma = 1.8 \times 10^{-19}$ cm^2 for the low-gain polarization and $\sigma = 6.1 \times 10^{-19}$ cm^2 for the high-gain polarization. It was not possible to measure these values to better than about 20%. They agree to better than 20% with data measured in Nd:LiNbO$_3$ by other authors.[7] However, these values are approximately three times larger than those extracted from fluorescence measurements (see Section 3), although the ratios of high- to low-gain cross sections are about the same in both measurements, namely, about 3.5. This disagreement has not yet been resolved but does not constitute a serious discrepancy for a quantity generally difficult to measure accurately. Laser characteristics certainly suggest that this material has a gain comparable with that of Nd:YAG under identical pumping arrangements.

5. PHOTOREFRACTIVE EFFECT

MgO doping has substantially reduced zero-field photorefractive damage. Previous reports on this effect in Nd:LiNbO$_3$ (Ref. 9) indicate a more severe problem than we observed. However, the photorefractive effect is still present despite the MgO doping. It also appears that Nd doping enhances this effect, as was previously noted in non-MgO-doped LiNbO$_3$.[5] It was ascertained that the damage was greater in the Nd-doped sample by visually comparing a Nd-doped and a non-Nd-doped sample after each was exposed to a focused 600-nm laser beam under similar conditions. A damage spot could be seen only in the Nd-doped sample. The damage spot could be annealed either by heating or by leaving the sample in room light for several hours.

In an attempt to obtain more quantitative results, we tried to form a photorefractive diffraction grating in the low-doped sample by intersecting two coherent pump beams at 514.5 nm. This diffraction grating was then probed by a laser beam at 632.8 nm. No diffraction could be observed with typical pump intensities of 1 W/cm^2. The instrument sensitivity placed an upper limit on the diffraction efficiency of about 10^{-5}. Previous reports indicate that diffraction gratings can be written into MgO:LiNbO$_3$ by using a similar technique[13] with 1-order-of-magnitude greater pump intensity.

In our experiments, the effect of photorefractive damage was to prevent true cw oscillation at room temperature in y-cut samples, whether for the π or σ polarization. However, quasi-cw oscillation was possible, as described earlier, with a duty cycle of 1.2%. At higher duty cycles degradation of the output power was observed, presumably caused by optical damage. At 33% duty cycle the output was reduced by a factor of 2. When the chopper was stopped, oscillation continued for 1–2 sec, then stopped. When the chopper was restarted, oscillation slowly returned over a period of 1–2 min.

On the other hand, as was previously mentioned, damage did not appear to affect true cw oscillation at room temperature in z-cut samples. Also, true cw oscillation was obtained in y-cut samples at elevated temperatures. For temperatures greater than 100 °C, damage had little or no effect on oscillation. As the temperature was continuously lowered from 100 °C, the photorefractive effect slowly became worse,

but true cw oscillation was obtained down to 50 °C for the π polarization and 30 °C in the σ polarization. The photorefractive damage appeared to be larger for the extraordinary index of refraction, as expected, since the damage is caused by index-of-refraction variations resulting from local electric fields coupling to the electro-optic effect. Since the r_{33} electrooptic coefficient of LiNbO$_3$ is relatively large compared with the other coefficients, one would expect the photorefractive damage to affect mainly the extraordinary index.

We hope to reduce this problem by investigating crystals with greater MgO doping and using semiconductor diode lasers as pump sources. It is hoped that greater MgO doping will offset the increase in photorefractive damage that is due to the addition of Nd, and semiconductor diode pumping will allow us to use longer pump wavelengths, for which the photorefractive response of the material is lower.

6. SELF-FREQUENCY DOUBLING

Self-frequency doubling offers the potential for efficient doubling because of the high intracavity intensities available in a simple system. We report here the first demonstration to our knowledge of cw self-frequency doubling. Previous demonstrations of self-frequency doubling have been in a pulsed mode.[3,10,24]

The experimental apparatus used for these measurements is essentially that described previously for cw laser operation. We chose to use 90° phase matching to avoid Poynting vector walk-off and obtain a higher conversion efficiency. To achieve 90° phase matching, the laser oscillation must be in the ordinary polarization (perpendicular to the z-axis), while the second-harmonic wave has an extraordinary polarization. Phase matching was achieved by temperature tuning the crystal birefringence. We therefore used a y-cut crystal that we placed in an oven. A Brewster angle window was inserted in the cavity to force the laser to oscillate in the σ polarization. Both cavity mirrors were 67% transmissive at the second-harmonic wavelength near 547 nm and highly reflective at the fundamental wavelength ($\lambda \sim 1.09 \ \mu$m). No attempt was made to oscillate the second harmonic, although it should be possible to increase the single-ended second-harmonic output by a factor of 4 if one of the cavity mirrors is made highly reflecting at the second-harmonic wavelength and if the proper phase relationship between the second harmonic and the fundamental required for second-harmonic generation is maintained in the crystal.[25] This fator-of-4 enhancement should be almost fully realizable in Nd:MgO:LiNbO$_3$, which has little absorption at the second-harmonic wavelength (unlike Nd:YAG or Nd:YLF).

Figure 6 shows the second-harmonic power generated in the forward direction as a function of dye-laser input power at a phase-matching temperature of about 152°C. The solid curve is a least-squares fit to a parabola. Twice as much second harmonic as indicated was actually generated because this figure is for single-ended output. Because of the high operating temperature the second-harmonic output was not limited by photorefractive damage, even up to the maximum power of 1 mW that we observed.

The conversion efficiency, defined as the ratio of total second-harmonic output to pump power absorbed above threshold, was 7.6% per watt. As mentioned above, this figure could be improved by making the laser cavity reso-
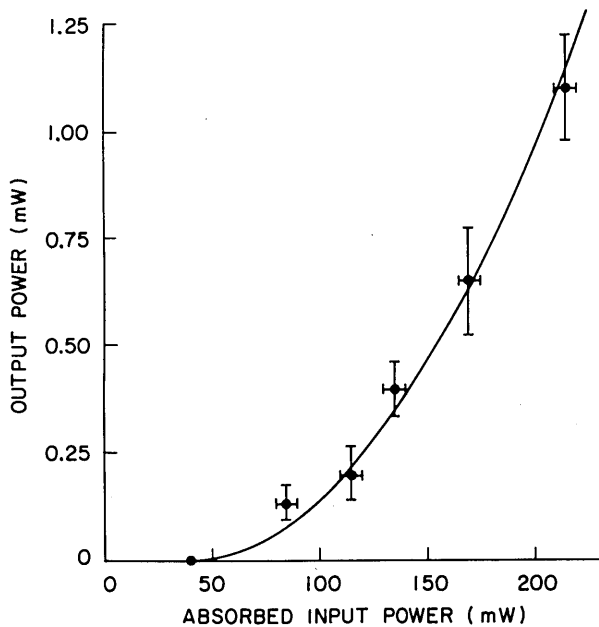
Fig. 6. Single-ended output at the second harmonic for the self-frequency-doubled laser.

nant at the second-harmonic wavelength and also by lowering the crystal loss and/or optimizing the crystal length. The efficiency of intracavity second-harmonic generation decreases rapidly with increasing intracavity loss[25] because of increasing threshold and lower cavity fluences for the fundamental. The sample used here had round-trip loss of about 2.3%. Improvement of the efficiency by at least 1 order of magnitude should be possible under optimum conditions.

Semiconductor diode pumping should also increase the efficiency. However, it is necessary to reduce the threshold by using lower-loss crystals and reducing phase-matching temperature before diode pumping becomes practical. We have found that at the phase-matching temperature the threshold is 2.3 times higher than at room temperature, which is consistent with previous results.[5] This could be due to a combination of (1) decreased stimulated-emission cross section because of thermally induced linewidth broadening, (2) increased lower laser level absorption, and (3) decreased fluorescence lifetime at elevated temperatures. Our lifetime-versus-temperature measurements rule out the last possibility, so the increased threshold is probably due to a combination of the first two effects. It appears possible to decrease the phase-matching temperature by increasing MgO doping[26]; however, clearly the crystal losses are of greater concern, and it is hoped that higher-quality crystals can be grown in the future.

7. ACTIVE INTERNAL Q SWITCHING

The term active internal Q switching is used in this paper to denote Q-switched operation in a laser in which the electro-optic (Pockels) cell and the active laser medium have been integrated into the same crystal rod. This Q-switching scheme offers the advantages over standard Q switching of miniaturization and reduced cavity loss. Our design of an internally Q-switched Nd:MgO:LiNbO$_3$ laser was based on the principle of cavity-loss modulation by means of a retardation plate and a polarizer, which is also the operation

principle of LiNbO$_3$ Q switches. These Q switches are usually operated as quarter-wave plates during the low-Q state for low switching voltage $V_{1/4}$. During the low-Q state radiation incident upon the crystal must be polarized at 45° to the crystallographic axes.

A detailed analysis of the possible crystal configurations for active internal Q switching was carried out assuming that the electro-optic tensor in LiNbO$_3$ was not modified appreciably by the Nd and MgO dopants. A result of the analysis was that x- and y-axis configurations are not suited for this type of Q switching. As discussed in previous sections, in x- and y-cut rods laser action is attained with the optical field being either parallel (π polarization) or orthogonal (σ) to z. A voltage applied to the crystal will change the state of polarization of this field only if it induces a rotation of the principal axes. However, the angle of rotation is either zero or exceedingly small even for voltages of the order of thousands of volts. On the other hand, in z-axis rods the lasing field can be forced to be linearly polarized at an arbitrary angle by means of an intracavity polarizer or a Brewster plate. In this case, applying an electric field parallel to the x-axis induces the required rotation of principal axes.

The experimental setup was the same as for the cw and quasi-cw measurements, except that we included the components shown in Fig. 3 by dashed lines. The miniature laser consisted of the long z-cut crystal in the nearly concentric cavity described in Section 4. Thin gold electrodes were deposited upon the side faces of the crystal, permitting the application of an electric field parallel to the crystal x axis. A thin Brewster window was inserted into the cavity to force the laser polarization also to be parallel to the crystal x axis. The chopper was replaced by an acousto-optic (A-O) cell, which modulated the pump into 500-μsec pulses at a repetition rate of 22 Hz.

A voltage pulse was applied to the crystal slightly before the beginning of each pump pulse to prevent quasi-cw oscillation. Switching this voltage to zero just before the end of the pump pulse resulted in the emission of a Q-switched pulse.

During pumping twice above threshold, a voltage of 250 volts was required to hold off quasi-cw oscillation. At this pump level the laser generated pulses 490-nsec wide (full width at half-maximum) with a peak power of 220 mW. When the Q-switched laser was operated at 4.5 times above threshold (110 mW of absorbed power), the pulse width was reduced to 250 nsec and the peak power was increased to 560 mW. The switching voltage was then 1000 V.

The measured pulse widths were compared with the predictions of Q-switched laser theory from the knowledge of the cavity loss δ. The cavity loss was deduced by using the method described in Section 4. We measured a quasi-cw slope efficiency of 8.4% and a threshold of 25 mW. From relation (6) we deduced that $\delta = 2.7\%$, which implies a minimum theoretical pulse width $\Delta t_{\min}$ of 30 nsec, equal to the photon lifetime inside the cavity. The Q-switched pulse widths Δt as a function of pump level $r = N_i/N_{\text{th}}$ can be calculated from[27]

$$\Delta t = \Delta t_{\min} \frac{r}{r - 1 - \ln r}, \tag{7}$$

where N_i is the population inversion just before the emission of the Q-switched pulse and N_{th} the threshold inversion. In

this equation, the final inversion N_f has been neglected. Assuming that $r \simeq P_{\text{abs}}/P_{\text{th}}$, we calculated pulse widths that coincide with the measured values within a factor of 3.

We tested the effect of an applied voltage on cw and quasi-cw laser operation after removing the Brewster plate from the cavity. With a duty cycle of 70% a cw voltage of about 500 V resulted in a reduction of the output power by a factor of 2/3. This problem was alleviated by reducing the duty cycle to $\approx 1\%$. These results suggest the presence of non-zero-field or electrically induced photorefractive damage.

We ascertained that an applied voltage of about 600 V was required to change the quasi-cw output polarization from linear to circular. This voltage is consistent with the measured minimum voltage of 250 V required to hold off quasi-cw oscillation during pumping twice above threshold. Although these results indicate an electro-optic coefficient r_{22} within a factor of 2 of that of congruent $LiNbO_3$, we believe the interpretation of these data may be questionable, as the internal electric field may have been affected by the electric field induced by photorefractivity. Further measurements using infrared radiations are required for r_{22} in this material to be determined without ambiguity.

The Q-switched laser that we operated demonstrates the potential of $Nd:MgO:LiNbO_3$ as a high-gain internally Q-switched laser material. The principle of cavity-loss modulation by a retardation plate and a polarizer was used in this device; nevertheless, other approaches are under investigation. A design based on an effective gain modulation instead of loss modulation will be particularly useful for x- and y-axis lasers. In these crystal configurations, zero-field photorefractive damage is also of concern, as discussed earlier, and further studies are required. Future efforts will concentrate also on the implementation of near-infrared pump sources to avoid zero-field and non-zero-field photorefractive damage.

8. CONCLUSION

Continuous-wave and quasi-cw laser oscillation near 1.09 μm has been demonstrated in miniature $Nd:MgO:LiNbO_3$ crystals end-pumped at 598 nm, with thresholds of the order of a few milliwatts and quantum efficiencies approaching the theoretical limit. In addition, we have demonstrated self-frequency doubled devices with up to 1 mW of cw output near 0.54 μm and the generation of 250-nsec, 560-mW peak-power pulses by using the electro-optical properties of the laser host to achieve internal Q switching. Analysis of the laser characteristics indicates gain cross sections of 6.1 $\times$ 10^{-19} cm^2 and 1.8 $\times$ 10^{-19} cm^2 for the high- and low-gain polarization, respectively. Although these values are higher than those deduced from independent spectroscopic measurements, they suggest that the optical gain of this material is comparable with that of Nd:YAG, which makes it a promising candidate for future solid-state devices.

One of the important results of this study is that the Nd and MgO dopants were found to have competing effects on the material's photorefractive properties. As a result, although the samples that we tested were far less susceptible to photorefractive damage than earlier samples that did not contain MgO, they still exhibited some degree of damage, which somewhat limited the performance of some devices.

However, the device characteristics were quite satisfactory and demonstrated the potential applications of this material as efficient solid-state lasers.

In the future, we hope to investigate the characteristics of samples with higher MgO doping levels to reduce photorefractive damage further and to lower the phase-matching temperature to achieve near-room-temperature self-frequency doubling. Also, efforts will be directed toward the implementation of semiconductor laser diodes as a pump source to reduce the material susceptibility to pump radiation and to increase the laser efficiency. Finally, a later step in this work may be the development of similar devices in a guided configuration, for example, in integrated-optic or crystal-fiber structures, to take advantage of a greater optical energy confinement and further improve the device efficiency.

ACKNOWLEDGMENTS

REFERENCES

1. N. F. Evlanova, A. S. Kovalev, V. A. Koptski, L. S. Kornienko, A. M. Prokhorov, and L. N. Rashkovich, "Stimulated emission of $LiNbO_3$ crystals with neodymium impurity," JETP Lett. **5**, 291 (1967).
2. L. I. Ivleva, A. A. Kaminskii, Y. S. Kuz'minov, and V. N. Shpakov, "Absorption, luminescence, and induced emission of $LiNbO_3–Nd^{3+}$ crystals," Sov. Phys. Dokl. **13**, 1185 (1969).
3. L. F. Johnson and A. A. Ballman, "Coherent emission from rare earth ions in electro-optic crystals," J. Appl. Phys. **40**, 297 (1969).
4. V. T. Gabrielyan, A. A. Kaminskii, and L. Li, "Absorption and luminescence spectra and energy levels of Nd^{3+} and Er^{3+} ions in $LiNbO_3$ crystals," Phys. Status Solidi (a) **3**, K37 (1970).
5. A. A. Kaminskii, "Laser and spectroscopic properties of activated ferroelectrics," Sov. Phys. Crystallogr. **17**, 198 (1972).
6. A. A. Kaminskii, "High temperature spectroscopic investigation of stimulated emission from lasers based on crystals activated with Nd^{3+} ions," Phys. Status Solidi (a) **1**, 573 (1970).
7. K. G. Belabaev, A. A. Kaminskii, and S. E. Sarkisov, "Stimulated emission from ferroelectric $LiNbO_3$ crystal containing Nd^{3+} and Mg^{2+} ions," Phys. Status Solidi (a) **28**, K17 (1975).
8. T. Y. Fan and R. L. Byer, "$Nd:MgO:LiNbO_3$ laser," in *Digest of the Conference on Lasers and Electro-Optics* (Optical Society of America, Washington, D.C., 1985), paper WJ4.
9. I. P. Kaminow and L. W. Stulz, "$Nd:LiNbO_3$ laser," IEEE J. Quantum Electron. **QE-11**, 306 (1975).
10. V. G. Dmitriev, E. V. Raevskii, N. M. Rubina, L. N. Rashkovich,

O. O. Silichev, and A. A. Fomichev, "Simultaneous emission at the fundamental frequency and the second harmonic in an active nonlinear medium: neodymium-doped lithium metaniobate," Sov. Tech. Phys. Lett. **4**, 590 (1979).

11. G. Zhong, J. Jian, and Z. Wu, "Measurements of optically induced refractive index damage of lithium niobate doped with different concentrations of MgO," In *Proceedings of the 11th International Quantum Electronics Conference*, IEEE Catalog No. 80CH 1561-0 (Institute of Electrical and Electronics Engineers, New York, 1980), p. 631.

12. H. Kai *et al.*, "Pure green laser applicable to high speed photography," presented at the 14th International Congress on High Speed Photography and Photonics, Moscow, October 19–24, 1980.

13. D. A. Bryan, R. Gerson, and H. E. Tomaschke, "Increased optical damage resistance in lithium niobate," Appl. Phys. Lett. **44**, 847 (1984).

14. A. Cordova-Plaza and M. J. F. Digonnet, "Self-Q-switched Nd:LiNbO$_3$ laser," J. Opt. Soc. Am. A **2**(13), P44 (1985).

15. G. Burns, D. F. O'Kane, and R. S. Title, "Optical and electron-spin resonance of Yb^{3+}, Nd^{3+}, and Cr^{3+} in $LiNbO_3$ and $LiTaO_3$," Phys. Rev. **167**, 314 (1968).

16. A. A. Kaminskii, *Laser Crystals* (Springer-Verlag, Berlin, 1981).

17. S. Singh, R. G. Smith, and L. G. VanUitert, "Stimulated emission cross-section and fluorescent quantum efficiency of Nd in yttrium aluminum garnet at room temperature," Phys. Rev. B **10**, 2566 (1974).

18. B. F. Aull and H. P. Jenssen, "Vibronic interactions in cross-sections," IEEE J. Quantum Electron. **QE-18**, 925 (1982).

19. T. S. Lomheim and L. G. DeShazer, "New procedure of determining neodymium fluorescence branching ratios as applied to 25 crystal and glass hosts," Opt. Commun. **24**, 89 (1978).

20. K. Kubodera, K. Otsuka and S. Miyazawa, "Stable LiNdP$_4$O$_{12}$ miniature laser," Appl. Opt. **18**, 884 (1979).

21. M. J. F. Digonnet and C. J. Gaeta, "Theoretical analysis of optical fiber laser amplifiers and oscillators," Appl. Opt. **24**, 333 (1985).

22. G. Huber, "Miniature neodymium lasers" in *Current Topics in Material Science*, E. Kaldis, ed. (North-Holland, Amsterdam, 1980), Vol. 4; M. J. F. Digonnet and H. J. Shaw, "Diode pumped fiber laser," Final Tech. Rep. AFWAL-F33615-82-C-1749 (June 1983).

23. H. G. Danielmeyer, in *Lasers: A Series of Advances*, A. K. Levine and A. DeMaria, eds. (Marcel-Dekker, New York, 1975), Vol. 4, p. 27.

24. L. M. Dorozhkin, I. I. Kuratev, N. I. Leonyuk, T. I. Timchenko, and A. V. Shestakov, "Nonlinear optical properties of neodymium yttrium aluminum borate crystals," Sov. Tech. Phys. Lett. **7**, 555 (1981).

25. R. G. Smith, "Theory of intracavity optical second harmonic generation," IEEE J. Quantum Electron. **QE-6**, 215 (1970).

26. W. Silva, Crystal Technology, 1035 East Meadow Circle, Palo Alto, Calif. 94303 (personal communication).

27. W. Koechner, *Solid State Laser Engineering* (Springer-Verlag, Berlin, 1976), p. 401.
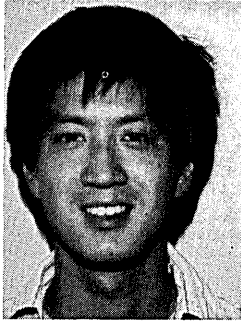
T. Y. Fan

T. Y. Fan was born in Manhattan, Kansas, in 1959. He received S.B. degrees from the Massachusetts Institute of Technology in both electrical engineering and materials science and engineering in 1981 and the M.S. degree in electrical engineering from Stanford University in 1983. Since 1983 he has been working toward a Ph.D., also in electrical engineering, at Stanford University. His research interests include new solid-state laser materials and devices and nonlinear optics.

A. Cordova-Plaza

A. Cordova-Plaza was born in Chiapas, México, on April 13, 1957. He received the B.S. degree with honors in physics from the Universidad Autónoma Metropolitana, México City, in 1979. In 1982 he received the *Diplôme d'Ingénieur* in electrical engineering and computer science from the Ecole Supérieure d'Electricité, Paris, and, in 1984, the M.S. degree in electrical engineering from Stanford University. In January 1979 he joined the research staff of the National Institute of Astrophysics, Optics and Electronics, Puebla, México, where he worked for one year in integrated circuit technology. At present he is a Ph.D. candidate at Stanford University in the fiber-optics group led by H. J. Shaw. His research interests include the design of miniature solid-state lasers for optical communications and other applications, the development of waveguide lasers and amplifiers, and integrated optics. He is a student member of the Optical Society of America.

M. J. F. Digonnet

M. J. F. Digonnet was born in Paris, France, in 1955. He received the engineering degree in physics and chemistry from l'Ecole Supérieure de Physique et de Chimie Industrielle de la Ville de Paris, Paris, France, and the *Diplôme d'Etude Approfondies* in optics from the University of Paris, Orsay, France, in 1978. He received the M.S. degree (1980) and the Ph.D. degree (1983), both in applied physics, from Stanford University, California. His graduate research included the development of single-mode fiber couplers and single-crystal fiber devices. Since then he has been with Litton Guidance and Control, Chatsworth, California, doing his research at Stanford University as a visiting scholar. His current research interests include single-crystal fibers for amplifier and source applications, miniature solid-state lasers, and the development of integrated-optics devices for optical-fiber sensors.

H. J. Shaw
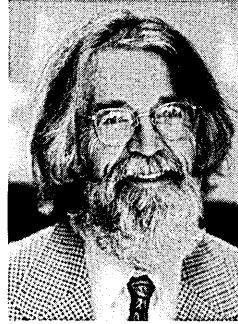
H. J. Shaw was born in Seattle, Washington, and received the B.A. degree from the University of Washington and the Ph.D. degree from Stanford University. He is a professor (research) at Stanford University. He has been engaged in research on microwave antennas and high-power microwave tubes, microwave ferrite devices involving resonance and spin waves, microwave acoustic devices including thin-film transducers, bulk wave delay lines and acousto-optic signal processors, and surface acoustic wave devices including transducers, delay lines, amplifiers, convolvers, matched filters and optical scanners. His present activities involve research on sensing and signal processing using optical fibers, on real-time acoustic imaging systems, and on piezoelectric polymer devices. He has been a consultant to a large number of electronic firms. During 1968–1969 he was liaison scientist for the U.S. Office of Naval Research in London. He is a member of Tau Beta Pi, a Fellow of the Institute of Electrical and Electronics Engineers (IEEE), and recipient of the 1976 Morris N. Liebmann Memorial Award of the IEEE "for contributions to the development of acoustic surface wave devices" and the 1981 Achievement Award of the IEEE Group on Sonics and Ultrasounds "for many contributions, through research and education, to ultrasonics technology."

R. L. Byer

R. L. Byer received the Ph.D. degree in applied physics in 1969 from Stanford University. His early and continuing interest has been in nonlinear interactions, including harmonic generation and parametric oscillators. After joining the Department of Applied Physics, Professor Byer initiated research into remote sensing using tunable laser sources. Research in that area led to the development of the unstable-resonator Nd:YAG laser and to high-power tunable infrared generation in $LiNbO_3$ parametric tuners. In 1974 he and his colleagues initiated research in coherent antistokes Raman spectroscopy, named the effect, and continued research in high-resolution Raman spectroscopy. In 1976 Professor Byer suggested the use of stimulated Raman scattering in hydrogen gas to generate 16-μm radiation from a CO_2 laser source. Research at Stanford University confirmed the expected simplicity and efficiency of the approach. In 1980 research on slab geometry solid state laser sources was initiated. The program has led to successful theoretical and experimental development in high peak and average power solid state laser sources. Research in advanced solid-state laser sources is continuing. He is a member of the American Association for the Advancement of Science and of the American Physical Society, a senior member of the Institute of Electrical and Electronics Engineers (IEEE), and a Fellow of the Optical Society of America and was president of the IEEE Lasers and Electro-Optics Society for 1985.